Characterization of particle exposure during tunnel excavation by tunnel boring machines

Torunn K. Ervik[1,*] [ID], Mimmi Leite[1], Stephan Weinbruch[1,2], Karl-Christian Nordby[1],
Dag G. Ellingsen[1], Bente Ulvestad[1], Kari Dahl[1], Balazs Berlinger[1,3], Nils Petter Skaugset[1]

[1]National Institute of Occupational Health, P.O. Box 5330, Majorstuen, 0304 Oslo, Norway
[2]Technical University of Darmstadt, Institute of Applied Geosciences, Schnittspahnstrasse 9, D-64287, Darmstadt, Germany
[3]Present address: Department of Animal Hygiene, Herd Health and Mobile Clinic, University of Veterinary Medicine, István u. 2.,
H-1078 Budapest, Hungary

*Corresponding author: Email: torunn.ervik@stami.no

Abstract

Tunnel boring machines (TBMs) are used to excavate tunnels in a manner where the rock is constantly penetrated with rotating cutter heads. Fine particles of the rock minerals are thereby generated. Workers on and in the vicinity of the TBM are exposed to particulate matter (PM) consisting of bedrock minerals including α-quartz. Exposure to respirable α-quartz remains a concern because of the respiratory diseases associated with this exposure. The particle size distribution of PM and α-quartz is of special importance because of its influence on adverse health effects, monitoring and control strategies as well as accurate quantification of α-quartz concentrations. The major aim of our study was therefore to investigate the particle size distribution of airborne PM and α-quartz generated during tunnel excavation using TBMs in an area dominated by gneiss, a metamorphic type of rock. Sioutas cascade impactors were used to collect personal samples on 3 separate days. The impactor fractionates the dust in 5 size fractions, from 10 µm down to below 0.25 µm. The filters were weighted, and the α-quartz concentrations were quantified using X-ray diffraction (XRD) analysis and the NIOSH 7500 method on the 5 size fractions. Other minerals were determined using Rietveld refinement XRD analysis. The size and elemental composition of individual particles were investigated by scanning electron microscopy. The majority of PM mass was collected on the first 3 stages (aerodynamic diameter = 10 to 0.5 µm) of the Sioutas cascade impactor. No observable differences were found for the size distribution of the collected PM and α-quartz for the 3 sampling days nor the various work tasks. However, the α-quartz proportion varied for the 3 sampling days demonstrating a dependence on geology. The collected α-quartz consisted of more particles with sizes below 1 µm than the calibration material, which most likely affected the accuracy of the measured respirable α-quartz concentrations. This potential systematic error is important to keep in mind when analyzing α-quartz from occupational samples. Knowledge of the particle size distribution is also important for control measures, which should target particle sizes that efficiently capture the respirable α-quartz concentration.

Key words: Tunnel excavation; TBM; quartz; particulate matter; impactor

---

What's Important About This Paper?

In this work size-fractionated concentrations of PM and α-quartz were measured during the operation of tunnel boring machines (TBMs) to excavate a tunnel in a gneiss-dominated area. All workers on the TBM were exposed to PM and α-quartz. Most PM and α-quartz mass was collected in the size range 10-0.5 µm and most respirable PM and α-quartz mass was calculated to be in the size range 2.5-1.0 µm. The α-quartz content in the samples varied between the sampling days, likely due to geological differences.

Introduction

In Norway, tunnels are excavated either by the conventional drill and blast method or by tunnel boring machines (TBMs). Where the drill and blast method uses explosives, TBMs use rotating cutter heads with cutter discs continually excavating the ground by indentation. Particulate matter (PM) containing fractions of the bedrock minerals are generated as the ground is excavated. The TBM can be visualized as an underground factory where the rock mass is transported on conveyor belts and removed from the tunnel. The tunnel is then lined with concrete segments at the back of the TBM to reinforce the tunnel wall and concrete and/or pea gravel is injected behind the segments. These processes involve different work tasks taking place simultaneously in the tunnel. Workers on the TBM may therefore be exposed to a variety of sources, including drilling, crushing, resuspension from conveyor belts, and backfilling when concrete linings are installed. However, additional sources of exposure may also be present.

Fine mineral particles are released into the tunnel when the TBM excavates the ground. In Norway, the bedrock is dominated by magmatic and metamorphic rocks like granite and gneiss, which consist of minerals like quartz, feldspar, muscovite, and biotite among others. Previous studies on exposure during TBM excavation reported respirable PM levels (geometric mean, GM) of 0.54 mg/m³ (Galea et al. 2015) and 0.42 mg/m³ (Leite et al. 2023), whereas a study conducted more than 20 years ago reported a GM of 2.0 mg/m³ (Bakke et al. 2001). The exposure levels for respirable crystalline silica, hereafter called α-quartz, for TBM workers, were reported in the latter 2 studies and were on average 59 μg/m³ (GM) and 39 μg/m³ (GM), respectively.

Exposure to respirable α-quartz in the lower airways may lead to diseases such as silicosis, chronic obstructive pulmonary disease, and lung cancer (IARC 2012). The particle size distribution of α-quartz as well as the composition of PM in different size ranges are important parameters for several reasons. First, the size of quartz particles is important for penetration and deposition efficiency in the respiratory tract and consequently the health responses in the lung (Mischler 2013; Ohyama et al. 2014; Chubb and Cauda 2017). Second, the accuracy of the analytical method for quantifying α-quartz in airborne samples depends on the size distribution (Gordon and Harris 1955; Stacey et al. 2009). Third, PM generated by crushing and grinding does not necessarily consist of the same composition as the rock itself. The airborne PM will also consist of other components, such as abrasives, smoke, and combustion particles, which do not originate from the bedrock (Sirianni et al. 2008). The particle size distribution and chemical composition may also vary with the work task (Cares et al. 1973; Sirianni et al. 2008). Knowledge of the size distribution and α-quartz content of PM of different size fractions is therefore beneficial for the development of effective monitoring and control strategies (Qi et al. 2016; Chubb and Cauda 2017).

The present investigation was conducted as a part of a larger study assessing exposure and health effects among TBM workers (Leite et al. 2023). The study was conducted in the Oslo region in Norway where the excavation of 2 parallel 20 km railroad tunnels started in 2015. The bedrock in this area consists of different types of Precambrian gneiss with lens-shaped bodies of amphibolite and pegmatite rocks (Graversen 1984; Gollegger 2018). In the coming years, tunnel excavation by TBMs is anticipated to increase. However, to the author's knowledge, there are no papers on the characterization of PM generated during tunnel excavation by TBMs. The present study is intended to fill this gap of knowledge by investigating the composition and particle size distribution of PM as well as the abundance and size distribution of α-quartz during tunnel excavation with TBMs.

Materials and methods

Sampling strategy

Four TBMs were used in the excavation process, each with a cutter head of 10 m diameter containing 71 cutter discs and a double-shielded electricity-driven 150 m long TBM body (Herrenknect AG, Schwanau, Germany). Personal air sampling with Sioutas impactors (SKC Inc., Eighty Four, PA, USA) was conducted in December 2018, and January and February 2019 at one of the 4 TBMs. A total of 15 personal samples were collected with Sioutas impactors across 3 sampling days spaced over the 3 months, with sampling times of 329 to 423 min. The following job functions were included in this study: cutter head mechanic, shield worker, segment crane operator, grouter, pipe worker, conveyor belt operator, and mechanic. Work tasks and location on the TBM are described elsewhere (Leite et al. 2023). To assess the size, morphology, and chemical composition of individual particles, one stationary short-time sampling was conducted with a Sioutas impactor at the front of the TBM to collect particles for scanning electron microscopy (SEM). In addition, 50 stationary respirable and thoracic samples were collected in parallel on the TBMs and in the tunnels behind the TBMs during the general exposure assessment performed in the study during 2017 to 2019.

Sampling equipment

A 5-stage Sioutas cascade impactor operated at a flow rate of 9 L/min maintained by SG 10-2 pumps (GSA

Messgerätebau GmbH, Ratingen, Germany) was used for personal sampling. Particles were collected in 5 size ranges: 10 to 2.5 µm, 2.5 to 1.0 µm, 1.0 to 0.5 µm, 0.5 to 0.25 µm, and <0.25 µm aerodynamic diameter (d_{ae}). The 4 coarser fractions were collected on 25 mm 0.5 µm pore size polytetrafluoroethylene (PTFE) filters (Pall Corporation, Port Washington, NY, USA), whereas particles on the after filter (<0.25 µm cutpoint) were collected on a 2.0 µm pore size 37 mm PTFE-filter (SKC Inc., Eighty Four, PA, USA). Due to an operational error, 1 personal Sioutas impactor sample was excluded. Additionally, 1 stationary sample was collected with the Sioutas impactor. In this case, the impactor was equipped with 3 mm diameter transmission electron microscopy (TEM) Cu-grids with holey carbon support films (EMresolution, Sheffield, UK) affixed to the PTFE filters to study the particles by scanning electron microscopy (SEM).

Parallel GK 2.69 thoracic (BGI Instruments, Waltham, MA, USA) and respirable cyclones (JS Holdings, Stevenage, UK) equipped with 37 mm diameter and 5 µm pore size polyvinylchloride (PVC) filters (Merck Millipore Ltd. Tullagreen, Cork, Ireland) were used for stationary sampling in the tunnels behind the TBMs and on the TBMs. The flow rate was 1.6 L/min and 2.2 L/min for thoracic and respirable cyclones, respectively. In total, 5 respirable and thoracic samples were excluded due to operational error or missing information on sampling time.

Gravimetry

The collected PM mass was determined by weighing all filters before and after exposure using a Sartorius MC-5 balance (Sartorius AG, Göttingen, Germany) with a readability of 0.001 mg in a temperature- and humidity-controlled room (20 ± 1 °C, 40 ± 2% relative humidity). The accuracy and precision of the mass determinations were assessed by weighing reference masses. The mass limit of detection (LOD) was 0.02 mg, calculated as 3 (SD) of all blank filters.

X-ray diffraction (XRD) analysis

The mass of α-quartz and other minerals on the filters was determined by X-ray diffraction (XRD) analysis with a Malvern Panalytical X'Pert³Powder diffractometer, equipped with an Empyrean X-ray Cu tube and a PIXcel[1D] detector (Malvern Panalytical B.V., Eindhoven, Netherlands). The α-quartz mass was quantified according to the NIOSH 7500 method (NIOSH 2003) using the NIST standard reference material (SRM) 2950a for calibration. This standard uses known amounts of NIST SRM 1878a respirable alpha quartz, deposited on 25 mm PVC filters. The LOD for the method was (3 * SD of all blank filters) 2 µg per filter. Prior to XRD analysis, the filters were treated

in a low-temperature plasma ashing (LTA) apparatus (Diener electronic GmbH & Co. KG, Ebhausen, Germany) to remove the filter substrate and organic material. The inorganic residue was filtrated onto a silver membrane filter with a pore size 0.45 µm (Merck Millipore Ltd. Tullagreen, Cork, Ireland). To investigate the mineral content of the samples a Rietveld refinement (Rietveld 1969) was performed on diffraction patterns from the first stage (d_{ae} = 10 to 2.5 µm) filter samples.

Scanning electron microscopy

Particles collected on TEM Cu-grids were investigated by SEM using a Hitachi SU6600 field emission instrument (Hitachi, Tokyo, Japan) equipped with a Bruker energy-dispersive X-ray (EDX) detector (Bruker Nano GmbH, Berlin, Germany). On each impactor stage, at least 500 particles were analyzed automatically using the Esprit Feature (Quantax version 1.9) software (Bruker Nano GmbH, Berlin, Germany). The whole particle was scanned during X-ray acquisition. The elemental composition (atomic %) was quantified with the standardless peak-to-background *ZAF* correction. Particle geometric properties such as for example projected area, Feret diameter, or equivalent projected area diameter were determined for each particle by the automatic particle analysis. In addition, some particles were mapped to investigate the elemental distribution within individual particles.

Size distribution calculations

It is possible to calculate the volume equivalent diameter (d_{ve}) as well as the d_{ae} from the equivalent projected area diameter (d_{pa}) if the volume shape factor (γ_p), dynamic shape factor (χ_p), and the density (ρ_p) of the particles are known (Davies 1979):

$$d_{ve} = d_{pa} \times \left(\frac{6 \times \gamma_p}{\pi} \right)^{\frac{1}{3}} \quad (1)$$

$$d_{ae} = d_{ve} \times \left(\frac{\rho_p}{\rho_0 \times \chi_p} \right)^{\frac{1}{2}} \quad (2)$$

Assuming that most of the PM is derived from the bedrock (gneiss), a density of 2.77 g/cm³ was used (Smithson 1971). This is an assumption because there may also be small contributions from other sources, including pea gravel or concrete. Based on previously reported values for quartz, a volume shape factor of 0.21 and a dynamic shape factor of 1.36 were applied (Cartwright 1962; Davies 1979). This is also merely an assumption since the PM will contain particles with various shape factors.

The geometric standard deviation (GSD) and the number median aerodynamic diameter (NMAD)

values were found from the cumulative size distribution, and thereafter the mass median aerodynamic diameter (MMAD) was calculated (Vincent 1995):

$$MMAD = NMAD \times \exp\left(3 \times \ln^2 GSD\right) \quad (3)$$

Air concentrations of respirable PM and α-quartz were calculated from the 5 size fractions collected by the Sioutas impactor and based on the convention curves for the respirable and thoracic fraction (Hinds 1982; ISO 1995), and as described by Berlinger et al. (2015). The GSD corresponding to the GM was calculated as the exponential of the standard deviation of the mean of the ln-transformed exposure variables. The MMAD for particle size distribution was calculated from the 2-point interpolation of data points representing the cumulative mass percent on either side of 50% (Christopher et al. 2010). The GSD is calculated by equation 4, where Dp (0.16) is found from 2-point interpolation of the data points representing the cumulative mass proportion above and below 0.16. Dp (0.84) is found from a 2-point interpolation of the data points representing the cumulative mass proportion above and below 0.84.

$$GSD = \sqrt{\frac{Dp\,(0.84)}{Dp\,(0.16)}} \quad (4)$$

The aerodynamic diameters for the NIST SRM 1878a were calculated based on the volume spherical diameters measured by light scattering given in the NIST certificate (NIST 2005) and can be calculated from equation 2, by using dynamic shape factor and density values for quartz of 1.36 and 2.6 g/cm^3, respectively. With these values, an MMAD of 2.2 µm and a GSD of 1.7 are obtained for the NIST SRM 1878a.

Statistical analysis

The associations between respirable PM and thoracic PM as well as between respirable α-quartz and respirable PM were assessed with the Theil-Sen estimator (Wilcox 2022), as the residuals in ordinary least squares regression were heteroscedastic and showed large deviations from a normal distribution. The differences in regression parameters for samples collected on the TBM and samples collected behind the TBM were tested with a basic bootstrap method (10.000 bootstrap samples) as advocated by Wilcox (2022). All calculations were performed with R version 4.1.2 (R-Core-Team, 2021) and using the Rallfun-v42 software (Wilcox 2022).

Results

PM and α-quartz concentrations collected with Sioutas impactors

The sum of all 5 impactor fractions (PM$_{10}$) led to PM and α-quartz mass concentrations (GM) of 693 µg/m^3 and 157 µg/m^3, respectively (Table 1). Generally, close to 50% of the PM mass was found in stage 1 ($d_{ae} = $ 10 to 2.5 µm) and more than 80% of the PM was found on the first 3 coarser particle size stages ($d_{ae} = $ 10-0.5 µm). The mass size distribution of α-quartz had

**Table 1.** Mass concentration (µg/m^3) of the particulate matter (PM) and α-quartz fractions collected with the Sioutas cascade impactor by personal sampling (n = 14). The calculated respirable fraction for the 5 stages is presented below the bold line. MMAD and GSD for the total and respirable fractions are included.

Size (µm)	PM (µg/m^3)						α-quartz (µg/m^3)					
	10 to 2.5	2.5 to 1.0	1.0 to 0.5	0.5 to 0.25	<0.25	Total	10 to 2.5	2.5 to 1.0	1.0 to 0.5	0.5 to 0.25	<0.25	Total
GM[a]	311	170	85	63	47	693	73	46	19	8.0	5.8	157
Minimum	158	82	39	33	18	412	44	16	5,9	2.7	2.4	81
Maximum	663	704	290	186	125	1915	291	323	113	52	21	792
90th	474	244	118	98	70	912	98	81	33	21	13	232
GSD[b]	1.5	1.6	1.5	1.5	1.7	1.4	1.6	2.0	1.9	2.2	1.9	1.7
MMAD[c]	2.4 (1.6 to 3.4) µm						2.4 (1.3 to 2.9) µm					
GSD	3.8						3.2					
Calculated respirable (GM)[a]	73	157	83	53	46	428	17	42	19	8	6	96
MMAD$_{resp}$[d]	1.2 (0.7 to 1.4) µm						1.4 (0.8 to 1.7) µm					
GSD$_{resp}$	3.3						2.6					

[a]Geometric mean, [b]Geometric standard deviation, [c]Mass median aerodynamic diameter for the collected PM given as GM with minimum and maximum values in parentheses, [d]Mass median aerodynamic diameter for the respirable fraction given as GM with minimum and maximum values in parentheses.

a similar profile to that of the PM (Supplementary Fig. S1) with similar MMAD and a slightly lower GSD (Table 1). All PM mass and α-quartz mass concentrations are shown in Supplementary Table S1. Due to the low number of samples, 14 samples collected on 3 different days including 7 different job functions, we refrained from testing. For PM and α-quartz, the computed respirable mass fraction was, on average (GM), 428 µg/m^3 and 96 µg/m^3 respectively (Table 1). A significant portion of the respirable mass fraction was collected in the 2.5-1.0 µm size range, with a PM and α-quartz concentration of 157 µg/m^3 and 42 µg/m^3, respectively.

The contribution of the total α-quartz to the total PM was on average 23%. However, the α-quartz percentage varied between the impactor stages and sampling days (Fig. 1). The α-quartz percentage on each Sioutas impactor stage was similar for the first 3 size
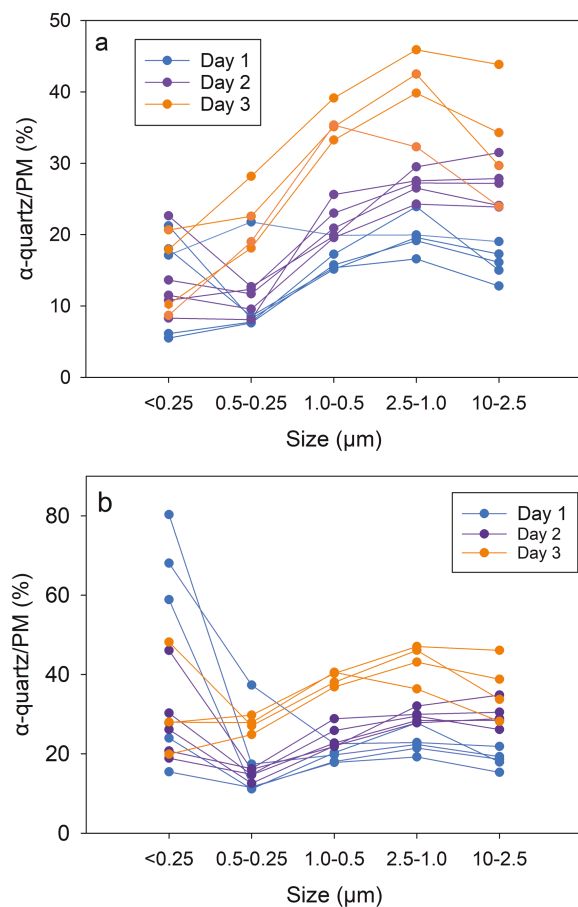
fractions (d_{ae} = 10 to 0.5 µm). The impactor stage 4 (d_{ae} = 0.5 to 0.25µm) had lower α-quartz content for 13 out of 14 samples, whereas for the after filter (d_{ae} < 0.25µm) 9 out of 14 samples had lower α-quartz content (Fig. 1a). When the mass after LTA was considered (Fig. 1b), the decrease for particles below 0.5 µm was less pronounced, whereas some after filters (<0.25 µm) had higher relative quartz contents than in the size fraction above (1.0 to 0.5 µm), in one case up to 80%. Samples collected on the same day showed comparable amounts of α-quartz.

The cumulative mass size distributions (personal samples) of respirable PM and α-quartz are similar (Fig. 2a and b). The cumulative mass size distribution of the NIST SRM 1878a is also plotted in Fig. 2b. The NIST SRM 1878a has a larger MMAD and a narrower particle size distribution than the estimated respirable distribution.
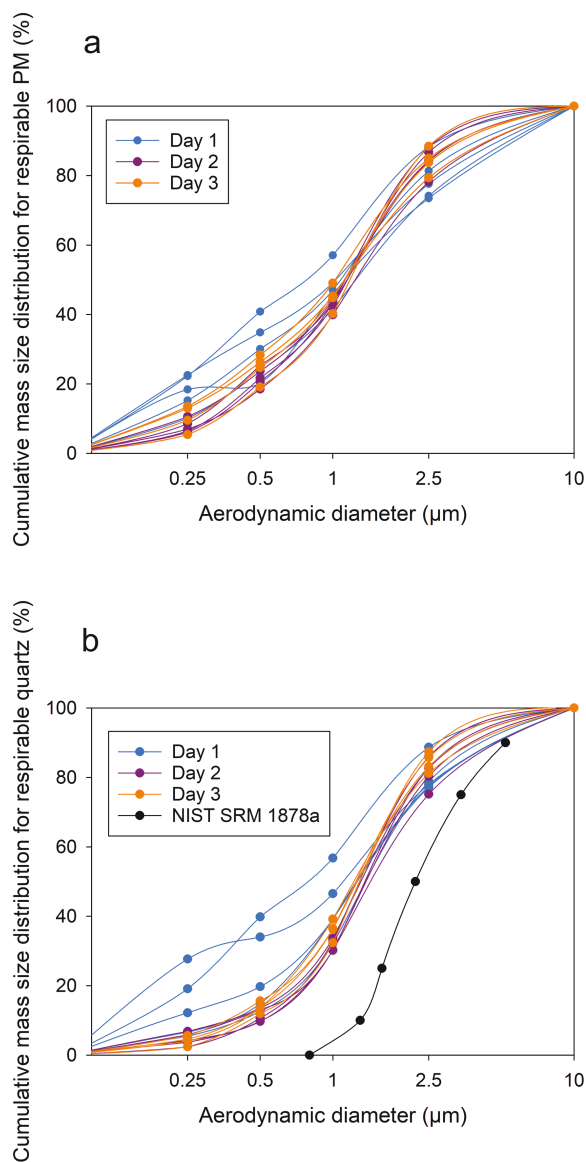
PM and α-quartz concentrations collected with stationary samples

Stationary samples collected behind the TBM (*n* = 38) had significantly lower thoracic and respirable PM concentrations than samples collected on the TBM (*n* = 11) (Fig. 3a). The respirable fraction was approximately 50 % of the thoracic fraction for both, samples collected on the TBM (median = 52%) and behind the TBM (median = 51%). The slope of the Theil-Sen estimator (Fig. 3a) is somewhat larger for samples collected on the TBM (2.96) than for samples collected behind the TBM (2.01). However, the slope difference is not statistically significant as judged from a percentile bootstrap method (*P* = 0.18).

The respirable α-quartz concentrations were also lower behind the TBM (*n* = 38) than on the TBM (*n* = 12) (Fig. 3b). The proportion of α-quartz in the respirable fraction is much higher for samples collected on the TBM (median = 19 %) than for samples collected behind the TBM (median = 6.9%). Here, the slope of the Theil-Sen estimator (Fig. 3b) is much larger for samples collected on the TBM (0.25) compared to samples collected behind the TBM (0.063). This slope difference is statistically significant (*P* = 0.0026).

Other minerals

The main mineral phases identified in the samples by XRD analysis on stage 1 filters (d_{ae} = 10 to 2.5 µm) were quartz, feldspar minerals (anorthite and microcline), calcite, biotite, and hornblende (Supplementary Table S2). Biotite is a common mineral within the mica group. The relative abundance of the major minerals varied between the 3 sampling days with α-quartz concentrations between 22 and 44 wt.%. Samples from Day 3 showed no hornblende in the Rietveld analysis, whereas microcline was observed. Samples from

Fig. 1. Relative α-quartz content (%) in each particle size fraction collected with the Sioutas cascade impactor by personal sampling before (a) and after low-temperature ashing (b). Sampling days are shown in different colors (*n* = 14).

Fig. 2. Particle mass size distribution (n = 14) of respirable PM (a) and respirable α-quartz (b) collected with the Sioutas cascade impactor by personal sampling. The cumulative size distribution of the NIST SRM 1878a is also plotted in (b).

persons 1 and 2 are lacking because the filters were cut and used for electron microscopy prior to XRD analysis.

Single particle analysis

Particles collected on the TEM Cu-grid fixed to PTFE filters in Sioutas were homogeneously distributed on the substrate and with a surface coverage that made automatic analysis feasible (Supplementary Fig. S2). The elements C, O, Si, Al, F, Na, Mg, K, Ca, Ti, Fe, and

Cu were detected by SEM-EDX. The elements Si and O were present in all mineral particles investigated. Carbon and Cu were also often detected due to the use of TEM Cu-grids covered with a supporting carbon film as substrate. Many particles were polymineralic consisting of more than one phase. One example is shown in Fig. 4. This particle consists predominantly of Si and O and is interpreted as quartz. The areas rich in Al, Ca, Fe, or Ti indicate the presence of inclusions of other minerals (e.g. Fe and Ti oxides). The variation of the chemical composition of mineral particles is shown as a ternary diagram (Supplementary Fig. S3). All particles with a (Na + Mg + Al + K + Ca + Ti + Fe)/Si ratio < 0.25 are classified as Si–O rich, as the histogram of this ratio (Supplementary Fig. S4 of the electronic supplement) shows a pronounced minimum at this value. This definition of Si–O-rich particles was previously used in the characterization of natural mineral dust (Scheuvens et al. 2011). These particles were interpreted as either pure quartz (if the ratio is very low) or as quartz-dominated agglomerates. The proportion of Si–O rich particles (plotting close to the Si corner of the ternary diagram) ranged from 19% to 28% (Table 2). Particles plotting along the Si–Al edge are most likely dominated by feldspar minerals, particles with more than a few percent Fe most likely by biotite or hornblende.

Size parameters obtained from the automated particle analysis and the equivalent projected area diameter were used to calculate the NMAD, MMAD, and the GSD of each impactor stage (Table 2). The calculated MMAD is within the nominal size range for impactor stage 1 (d_{ae} = 10 to 2.5 μm) and impactor stage 2 (d_{ae} = 2.5 to 1.0 μm). However, for stage 3 (d_{ae} = 1.0 to 0.5 μm), stage 4 (d_{ae} = 0.5 to 0.25 μm), and the after filter (d_{ae} < 0.25 μm) the MMAD values found by SEM exceed the nominal size range given by the manufacturer. The NMAD for all stages was below 1 μm.

Discussion

PM and α-quartz air concentrations and particle size distribution

In the present study, the PM size distribution was found to have a similar profile for the different job functions measured (Supplementary Fig. S1a). A greater variation in the particle size distribution of personal samples may be anticipated when actively using handheld equipment on rocks, as was found when investigating particle size distribution in granite quarry dust (Sirianni et al. 2008). On the TBM a more homogenous situation may be expected as the workers are all working in the same environment and the primary tool is the rotating cutter disc indenting the rock up front. Still, several factors may influence the particle
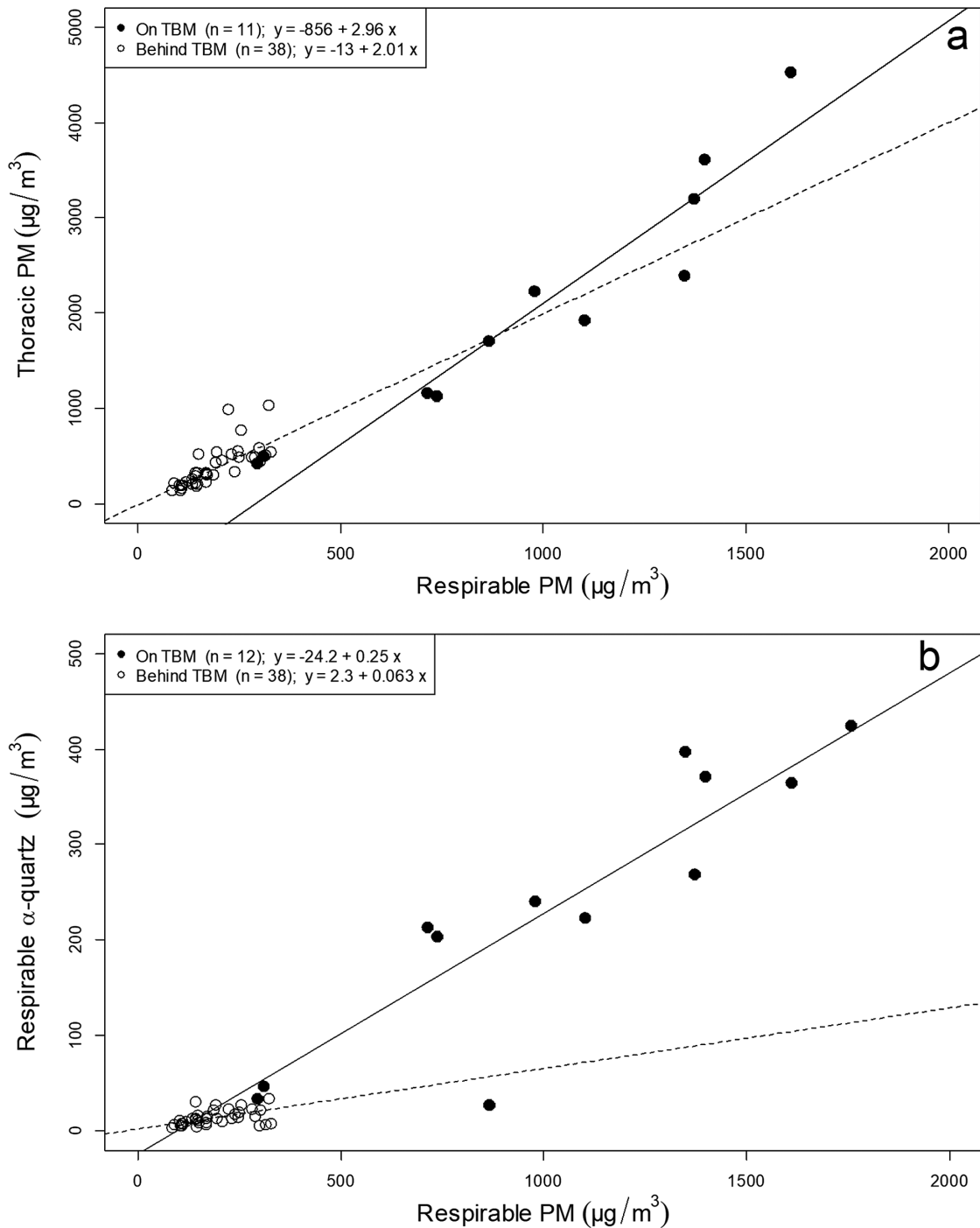
Fig. 3. Association between thoracic and respirable mass concentrations for stationary samples (a), and between respirable α-quartz and respirable mass concentration (b) for stationary samples.

size distribution such as bedrock composition, drilling activities, wear of cutter discs, and operational parameters (Yang et al. 2020). Other activities taking place on the TMB, such as welding, may also influence particle size distribution. The slightly narrower size distribution for α-quartz (GSD = 3.2) compared to the PM
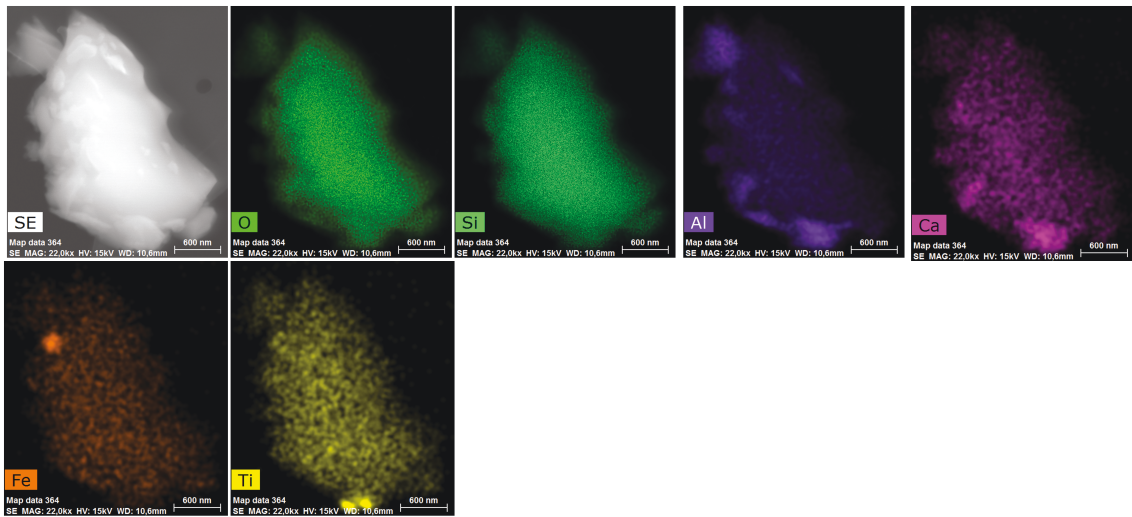
Fig. 4. Secondary electron (SE) and element distribution images of a particle collected on stage 1 (d_{ae} = 10 to 2.5 µm) in the Sioutas impactor. The scale bars equal 600 nm.

(GSD = 3.8) may result from α-quartz originating from rocks, either bedrock or pea gravel used in concrete lining, whereas the general dust is also affected by all other sources in the tunnel (Chubb and Cauda 2017).

The total mass concentration from the 5 Sioutas stages (Table 1) was 693 µg/m³ (GM), which is comparable to the thoracic mass fraction of 710 µg/m³ (GM) found by Leite et al. (2023) for all job titles. The PM$_{10}$ and thoracic size fractions are similar up to about 12 µm where the 2 curves diverge (Brown et al. 2013), and the thoracic fraction may contain particles up to 40 µm. Bau and Witschger (2013) estimated the deposition efficiency of the Sioutas impactor to be as high as about 90% for d_{ae} = 40 µm with decreasing deposition probability to about 10% for d_{ae} 80 µm. The similarity of the total Sioutas mass and the thoracic mass reported by Leite et al. (2023) indicates that few very large particles were present. In the tunnel, it is expected that most workers are located at some distance away from the PM and α-quartz generating source and that the largest particles sediment to the ground before reaching the workers breathing zone.

The calculated respirable fractions of PM and α-quartz, 428 µg/m³ and 96 µg/m³ respectively, from the Sioutas impactor (Table 1) are in the same range as the concentrations found by Leite et al. (2023) for personal samples (GM of 420 µg/m³ and 59 µg/m³ for respirable PM and respirable α-quartz, respectively). Most of the respirable α-quartz mass is found in stage 2 with d_{ae} = 2.5 to 1.0 µm. Similar size distributions for respirable α-quartz were obtained for cutting fiber cement sidings (Qi et al. 2016) and for aerosolizing gold mine dust in a laboratory (Chubb and Cauda 2017). In a study

investigating griding of engineered stones, however, the highest generation rate of respirable α-quartz occurred at 3.2 to 5.6 µm (Thompson and Qi 2022). Fine particles penetrate deeper into the lungs than coarse particles. With respect to deposition, particle diameters of 2.5 to 1.0 µm have an increased deposition efficiency compared to smaller particle diameters between 0.1 and 1 µm (Bartley and Vincent, 2011; Braakhuis et al., 2014). On the other hand, smaller particles are likely to cause more lung effects than equivalent masses of larger particles because they have a larger surface area per unit mass than larger particles (Meldrum and Howden, 2002). Crystalline silica particles with a size of 0.3 µm (GM) were found to enhance the activation of alveolar macrophages compared to larger particles (Mischler et al., 2016).

The relative abundance of α-quartz in the 3 first stages (d_{ae} = 10 to 0.5 µm; Fig. 1a) varied between 13 to 20% (Day 1), 20 to 31% (Day 2), and 28 to 44% (Day 3). These levels are within the range of α-quartz abundance reported in the bedrock. Thus, the differences seen between the 3 sampling days may be explained by variations in the composition of the bedrock. Unfortunately, no rock samples were collected on the 3 sampling days and the exact mineral composition of the bedrock is therefore not known. The Rietveld method also showed differences in α-quartz content between the 3 sampling days (Supplementary Table S2) with similar percentages as found by NIOSH 7500 method (Fig. 1). Leite et al. (2023) noted in their work that the variation between different days was larger for α-quartz than for respirable PM also indicating an effect of the bedrock composition. The presence

Table 2. Size parameters of particles from automatic SEM analysis and the proportion of Si–O rich particles.

Impactor stage cut size (µm)	Equivalent projected area diameter d_{pa}				NMAD (µm)	GSD	MMAD$_{calc}$ (µm)	% Si–O-rich particles
	AM	Min.	Max.	SD				
10 to 2.5 (n = 800)	1.2	0.32	9.4	1.0	0.87	2.2	5.4	26
2.5 to 1.0 (n = 626)	1.3	0.25	9.2	1.1	0.83	1.8	2.1	26
1.0 to 0.5 (n = 1012)	0.69	0.25	3.1	0.38	0.62	1.7	1.6	28
0.5 to 0.25 (n = 876)	0.61	0.25	3.9	0.37	0.52	1.6	0.95	20
<0.25 (n = 587)	0.34	0.21	1.7	0.14	0.32	1.3	0.41	19

of Hornblende indicates amphibolite in the bedrock. Knowing the composition of the PM is important since other components in the dust may also have negative health impacts. Mica dust for instance is known to cause fibrosis (Zinman et al. 2002). Recent studies on pro-inflammatory effects and cytotoxicity of mineral dusts and respirable rock particles emphasize the need for further attention on sheets-like mica minerals like muscovite and biotite. (Grytting et al. 2021, 2022).

From Fig. 1 it can be seen that the α-quartz content decreased for stage 4 and the after filter for many of the samples. Hall et al. (2021) reported results with quartz concentrations consistent with the bulk material in the size range from 0.5 to 1.0 µm and upwards when using Sioutas impactors during the cutting of sandstone, granite, and artificial stones in a dust tunnel facility. In real workplace measurements, it may be expected that the α-quartz proportion decreases with a smaller aerodynamic diameter because of increasing fraction of other types of PM, generated from combustion processes rather than mechanical generation. Diesel-powered vehicles were used inside the tunnel to transport workers and equipment to the TBM. Diesel soot particles will occur in the 2 smallest size bins of the Sioutas impactor (Kittelson and McMurry 2004). In addition, workers on the TBM were observed to smoke in the tunnel and some of the after filters collected on the TBM appeared slightly yellow. The higher organic matter content was shown by a higher mass loss after the LTA procedure (Fig. 1b). A study of the particle size distribution of exhaled cigarette smoke has shown that most particles are in the size range 200 to 250 nm (Braun et al. 2019), which fits well with the cut point for stage 4 (d_{ae} = 0.5 to 0.25 µm) and below in the impactor.

However, even after the organic content is removed, there is still a decrease in α-quartz content for stage 4 (d_{ae} = 0.5 to 0.25 µm) (Fig. 1b). This may be caused by a decreased XRD measurement response for particles less than 1 µm. This effect is due to a small amorphous layer of about 0.03 µm thickness on the α-quartz

particle surface, which contributes increasingly to the particle volume and mass with decreasing particle size (Dempster and Ritchie 1952; Nagelschmidt et al. 1952; Page 2003; Stacey et al. 2021). Consequently, the particle size distributions of the calibration material and the workplace should be matched (Stacey et al. 2009). The SRM used for calibration (NIST SRM 1878a) has a higher MMAD and a smaller GSD (Fig. 2) than the respirable α-quartz collected in the tunnel. Hence, a larger number of small particles below 1 µm diameter exists in the collected α-quartz compared to the NIST SRM. Furthermore, it should be mentioned that previous studies measuring the NIST SRM 1878a particle size revealed volume median diameters of 2.27 and 2.5 µm, deviating from the 1.6 µm value specified in the NIST certificate (Kauffer et al. 2003; Stacey et al. 2009). This will further result in increased MMAD of the NIST SRM and a possible larger discrepancy from the measured particle size distribution. Correction factors for the stages in the Sioutas impactor can be developed to account for the lower XRD response using a method described in Stacey et al. (2021). The effect of the lowered response is largest at the 2 final stages (d_{ae} > 0.5 µm), where the mass concentration of PM is likewise lowest. Nevertheless, the effect should be considered in future work as it has implications for the α-quartz concentrations.

The dramatic increase of α-quartz abundance on some of the after filters is most likely caused by larger particles bouncing off upper stages.

PM and α-quartz concentrations collected with stationary samplers

The stationary samples on the TBM were all collected close to the TBM front where the PM and α-quartz concentrations were reported to be highest for personal samples (Leite et al. 2023). The distribution of stationary samples collected on the TBM will therefore be in favor of higher PM concentrations. The respirable fraction was approximately 50% of the thoracic, both on the front and behind the TBM, and

demonstrates that the size distribution of dust was similar. However, the respirable α-quartz content is quite different: 19% on the TBM front and 6.9% in the tunnel behind the TBM. In the latter case, the samples are collected further away from the α-quartz source and are, therefore, diluted with other types of PM that contain less or no α-quartz. On the other hand, given that cross passageways between the parallel tunnels were constructed using the drill and blast technique, the samples collected behind the TBM may have been impacted by such operations. Unfortunately, drill and blast incidents were not registered, therefore it is unknown if the stationary samples were exposed to such occurrences.

Analysis of individual particles by SEM

Most particles were mineral particles with an irregular shape generated from the impaction and crushing of the bedrock. Combustion particles such as soot agglomerates were also found by SEM. The automated analysis yielded a relative number abundance between 19% and 28 % for Si–O rich particles for the 5 size fractions collected by the Sioutas impactor. A decrease in the proportion of α-quartz for stage 4 (d_{ae} = 0.5 to 0.25 μm) and after the filter (d_{ae} < 0.25 μm) is observed (Table 2). In SEM-EDX this decrease cannot be explained by any reduction in measurement response. Instead, it is most likely caused by the presence of other particle groups, such as combustion particles with low atomic numbers (please note that relative number abundances are compositional data with a constant sum).

The calculated MMAD is higher than the nominal size intervals for stage 3 (d_{ae} = 1.0 to 0.5 μm) and stage 4 (d_{ae} = 0.5 to 0.25 μm) which may be explained by a systematic underestimation of carbon-rich particles due to their lower contrast in backscatter electron (BSE) images. The BSE image is used in the automated analysis to recognize the particles, and particles with an average low atomic number have a low contrast. Consequently, the abundance of combustion particles, mainly found on stage 4 and after filter, is likely to be underestimated. It should be emphasized here that the calculation of MMAD from SEM data only yields a rough estimate. The dynamic shape factor and the volume shape factor were values for quartz and were used for all particles measured by SEM. Biotite, which is a mica mineral, has probably the largest effect since micas are plate-liked particles. Studies on talc, which has the similar plate-like shape to micas, yield a volume shape factor of 0.075 and a dynamic shape factor of 1.88 (Cheng et al. 1988). The influence of many plate-like particles could influence the calculated aerodynamic diameters in Table 2 in the direction of smaller MMADs.

Strength and limitations

Since access to this kind of workplace is difficult, the study's strongest point is the unique collection of personal size-fractionated samples in this environment. However, more samples would have been beneficial for identifying larger variances between days and workers. Collecting parallel respirable cyclones would be useful for comparing the calculated respirable fraction from the Sioutas impactors. Collecting material samples from the bedrock and pea gravel would also be beneficial to estimate the α-quartz content as well as other minerals in the rocks.

Conclusion

Similar size distribution profiles were found for PM and α-quartz collected on TBM workers using Sioutas impactors during 3 separate collection days. Most of the respirable α-quartz mass is found in the size range d_{ae} = 2.5 to 1.0 μm. Knowing the particle size distribution is important for designing preventive measures to minimize worker's exposure to respirable α-quartz. During the course of the 3 sampling days, the α-quartz fraction varied, indicating a geological dependence. Knowing the α-quartz content in the bedrock is therefore highly important. Other minerals detected in the PM, such as biotite, can also pose negative health effects and should be included in future exposure characterization studies. The number of particles smaller than 1 μm in the collected α-quartz was higher than in the calibration material, which may have an impact on the accuracy of respirable α-quartz concentration measurements.

Conflict of interest

The authors declare no conflict of interest relating to the material presented in this article. Its contents, including any opinions and/or conclusions expressed, are solely those of the authors.

Disclaimer

Bane-Nor did not play any role in the design of the study; in the collection, preparation, analysis, and interpretation of the data; in writing this article; or in the decision to submit this paper for publication.

Data availability

The data underlying this article will be shared on reasonable request to the corresponding author.

Supplementary material

Supplementary material is available at *Annals of Work Exposures and Health* online.

References

NIOSH. Silica, crystalline, by XRD (filter redeposition) Cincinnati, OH, USA: NIOSH Manual of Analytical Methods NMAM; 2003.

Bakke B, Stewart P, Ulvestad B, Eduard W. Dust and gas exposure in tunnel construction work. AIHAJ: J Sci Occup Environ Health Safety. 2001:62(4):457–465. https://doi.org/10.1080/15298660108984647

Bau S, Witschger O. A modular tool for analyzing cascade impactors data to improve exposure assessment to airborne nanomaterials. J Phys Conf Ser. 2013:429:012002. https://doi.org/10.1088/1742-6596/429/1/012002

Berlinger B, Bugge MD, Ulvestad B, Kjuus H, Kandler K, Ellingsen DG. Particle size distribution of workplace aerosols in manganese alloy smelters applying a personal sampling strategy. Environ Sci Process Impacts. 2015:17(12):2066–2073. https://doi.org/10.1039/c5em00396b

Bartley DL, Vincent JH. Sampling Conventions for Estimating Ultrafine and Fine Aerosol Particle Deposition in the Human Respiratory Tract. *Ann Occup Hyg*. 2011:55(7):696–709. https://doi.org/10.1093/annhyg/mer037

Braun M, Koger F, Klingelhöfer D, Müller R, Groneberg DA. Particulate matter emissions of four different cigarette types of one popular brand: influence of tobacco strength and additives. Int J Environ Res Public Health. 2019:16(2):263. https://doi.org/10.3390/ijerph16020263

Brown JS, Gordon T, Price O, Asgharian B. Thoracic and respirable particle definitions for human health risk assessment. Part Fibre Toxicol. 2013:10(1):12. https://doi.org/10.1186/1743-8977-10-12.

Braakhuis HM, Park MVDZ, Gosens I, De Jong WH, and Cassee FR. Physicochemical characteristics of nanomaterials that affect pulmonary inflammation. *Part Fibre Toxicol*. 2014:11(1):18. https://doi.org/10.1186/1743-8977-11-18

Cares JW, Goldin AS, Lynch JJ, Burgess WA. The determination of quartz in airborne respirable granite dust by infrared speetrophotometry. Am Ind Hyg Assoc J. 1973:34(7):298–305. https://doi.org/10.1080/0002889738506850

Cartwright J. Particle shape factors. Ann Occup Hyg. 1962:5(3):163–171. https://doi.org/10.1093/annhyg/5.3.163

Cheng Y-S, Yeh H-C, Allen MD. Dynamic shape factor of a plate-like particle. Aerosol Sci Technol. 1988:8(2):109–123. https://doi.org/10.1080/02786828808959176.

Christopher JD, Dey M, Lyapustina S, Mitchell J, Tougas TP, Oort M, Strickland H, Wyka B, Zaidi K. Generalized simplified approaches for mass median aerodynamic determination. Pharm J. 2010:36(3):812–823.

Chubb LG, Cauda EG. Characterizing particle size distributions of crystalline silica in gold mine dust. Aerosol Air Qual Res. 2017:17(1):24–33. https://doi.org/10.4209/aaqr.2016.05.0179

Davies CN. Particle-fluid interaction. J Aerosol Sci. 1979:10(5):477–513. https://doi.org/10.1016/0021-8502(79)90006-5

Dempster PB, Ritchie PD. Surface of finely-ground silica. Nature. 1952:169(4300):538–539. https://doi.org/10.1038/169538b0

Galea KS, Mair C, Alexander C, de Vocht F, van Tongeren M. Occupational exposure to respirable dust, respirable crystalline silica and diesel engine exhaust emissions in the london tunnelling environment. Ann Occup Hyg. 2015:60(2):263–269. https://doi.org/10.1093/annhyg/mev067

Gollegger J. Experience from TBM excavation obtained in the Follo Line Project. Geomech Tunnel. 2018:11(5):487–491. https://doi.org/10.1002/geot.201800024

Gordon RL, Harris GW. Effect of particle-size on the quantitative determination of quartz by x-ray diffraction. Nature. 1955:175(4469):1135–1135. https://doi.org/10.1038/1751135a0.

Graversen O, Geology and structural evolution of the Precambrian rocks of the Oslofjord-Øyeren area, Southeast Norway. Vol. Bulletin 398. Trondheim, Norway: Geological Survey of Norway; 1984.

Grytting VS, Refsnes M, Låg M, Erichsen E, Røhr TS, Snilsberg B, White RA, Øvrevik J. The importance of mineralogical composition for the cytotoxic and pro-inflammatory effects of mineral dust. Part Fibre Toxicol. 2022:19(1):46. https://doi.org/10.1186/s12989-022-00486-7

Grytting VS, Refsnes M, Øvrevik J, Halle MS, Schönenberger J, van der Lelij R, Snilsberg B, Skuland T, Blom R, Låg M. Respirable stone particles differ in their ability to induce cytotoxicity and pro-inflammatory responses in cell models of the human airways. Part Fibre Toxicol. 2021:18(1):18. https://doi.org/10.1186/s12989-021-00409-y

Hall S, Stacey P, Pengelly I, Stagg S, Saunders J, Hambling S. Characterizing and comparing emissions of dust, respirable crystalline silica, and volatile organic compounds from natural and artificial stones. Ann. Work Expo. Health. 2021:66(2):139–149. https://doi.org/10.1093/annweh/wxab055

Hinds WC, Aerosol technology: properties, behavior, and measurement of airborne particles. New York, USA: Wiley; 1982.

IARC. Silica dust, crystalline, in the form of quartz or cristobalite. Lyon, France: International Agency for Research on Cancer; 2012.

ISO. ISO 7708 Air quality-particle size fraction definition for health-related sampling. 1995, International Standard Organization

Kauffer E, Martin P, Grzebyk M, Villa M, Vigneron JC. Comparison of two direct-reading instruments (FM-7400 and Fibrecheck FC-2) with phase contrast optical microscopy to measure the airborne fibre number concentration. Ann Occup Hyg. 2003:47(5):413–426. https://doi.org/10.1093/annhyg/meg055

Kittelson DB, McMurry PH. Structural properties of diesel exhaust particles measured by Transmission Electron Microscopy (TEM): relationships to particle mass and mobility AU - Park, Kihong. Aerosol Sci Technol. 2004:38(9):881–889. https://doi.org/10.1080/027868290505189

Leite M, Nordby K-C, Skare O, Ulvestad B, Ellingsen DG, Dahl K, Johansen T, Petter Skaugset N. Exposure to particulate matter and respirable crystalline silica in tunnel construction workers using tunnel boring machines. Ann Work Expo Health. 2023:67(5):584–595. https://doi.org/10.1093/annweh/wxad004

Meldrum M, Howden P. Crystalline Silica: Variability in Fibrogenic Potency. The Annals of Occupational Hygiene. 2002:46(suppl_1):27–30. https://doi.org/10.1093/annhyg/46.suppl_1.27

Mischler SE, A multistage cyclone array for the collection of size-segregated silica aerosols to test the hypothesis that ultrafine crystalline silica particles are more efficient in their activation of macrophages, in the Graduate School of Public Health. University of Pittsburgh; 2013.

Mischler SE, Cauda EG, Di Giuseppe M, McWilliams LJ, St. Croix C, Sun M, Franks J, and Ortiz LA. Differential activation of RAW 264.7 macrophages by size-segregated crystalline silica. *J Occup Med Toxicol.* 2016:11(1):57. https://10.1186/s12995-016-0145-2

Nagelschmidt G, Gordon RL, Griffin OG. Surface of finely-ground silica. Nature. 1952:169(4300):539–540. https://doi.org/10.1038/169539a0

NIST, Standard Reference Material 1878a. Gaitherburg, MD, USA: National Institute of Standards and Technology; 2005.

Ohyama M, Tachi H, Minejima C, Kameda T. Comparing the role of silica particle size with mineral fiber geometry in the release of superoxide from rat alveolar macrophages. J Toxicol Sci. 2014:39(4):551–559. https://doi.org/10.2131/jts.39.551

Page SJ. Comparison of coal mine dust size distributions and calibration standards for crystalline silica analysis. AIHA J Sci Occup Environ Health Safety. 2003:64(1):30–39. https://doi.org/10.1080/15428110308984781

Qi C, Echt A, Gressel MG. On the characterization of the generation rate and size-dependent crystalline silica content of the dust from cutting fiber cement siding. Ann Occup Hyg.

2016:60(2):220–230. https://doi.org/10.1093/annhyg/mev066

R-Core-Team. A language and environment for statistical computing. 2021; Available from: https://www.R-project.org/

Rietveld HM. A profile refinement method for nuclear and magnetic structures. J Appl Crystallogr. 1969:2(2):65–71. https://doi.org/10.1107/s0021889869006558

Scheuvens D, Kandler K, Küpper M, Lieke K, Zorn SR, Ebert M, Schütz L, Weinbruch S. Individual-particle analysis of airborne dust samples collected over Morocco in 2006 during SAMUM 1. Tellus B. 2011:63(4):512–530. https://doi.org/10.1111/j.1600-0889.2011.00554.x

Sirianni G, Hosgood HD, Slade MD, Borak J. Particle size distribution and particle size-related crystalline silica content in granite quarry dust. J Occup Environ Hyg. 2008:5(5):279–285. https://doi.org/10.1080/15459620801947259

Smithson SB. Densities of metamorphic rocks. Geophysics. 1971:36(4):690–694. https://doi.org/10.1190/1.1440205

Stacey P, Hall S, Stagg S, Clegg F, Sammon C. Raman spectroscopy and X-ray diffraction responses when measuring health-related micrometre and nanometre particle size fractions of crystalline quartz and the measurement of quartz in dust samples from the cutting and polishing of natural and artificial stones. J Raman Spectrosc. 2021:52(6):1095–1107. https://doi.org/10.1002/jrs.6110

Stacey P, Kauffer E, Moulut JC, Dion C, Beauparlant M, Fernandez P, Key-Schwartz R, Friede B, Wake D. An international comparison of the crystallinity of calibration materials for the analysis of respirable alpha-quartz using X-ray diffraction and a comparison with results from the infrared KBr disc method. Ann Occup Hyg. 2009:53(6):639–649. https://doi.org/10.1093/annhyg/mep038.

Thompson D, Qi C. Characterization of the emissions and crystalline silica content of airborne dust generated from grinding natural and engineered stones. Ann. Work Expo. Health. 2022:67(2):266–280. https://doi.org/10.1093/annweh/wxac070

Vincent JH, Chapter 3—properties of aerosols. In:, Vincent JH, editor. Aerosol science for industrial hygienists Pergamon: Amsterdam, Netherlands; 1995. p. 37–71.

Wilcox RR, Introduction to robust estimation and hypothesis testing. 5th ed. London, UK: Academic Press; 2022.

Yang X, Elsworth D, Zhou J, Nie A, Liu L. A new approach to evaluate the particle size distribution from rock drilling: double peak characteristic analysis. Geomech Geophys Geo-Energy Geo-Resources. 2020:6(2):38. https://doi.org/10.1007/s40948-020-00161-1

Zinman C, Richards GA, Murray J, Phillips JI, Rees DJ, Glyn-Thomas R. Mica dust as a cause of severe pneumoconiosis. Am J Ind Med. 2002:41(2):139–144. https://doi.org/10.1002/ajim.10032